Design and wind tunnel test of a MODular aeroelastic FLEXible wing (MODFLEX)

S. Fichera[1], S. Jiffri[1] and J. E. Mottershead[1]
[1] University of Liverpool, School of Engineering
Liverpool, L69 3GH, United Kingdom
e-mail: **sebastiano.fichera@liverpool.ac.uk**

Abstract
The paper presents the design, development and experimental validation of the MODular aeroelastic FLEXible wing for wind tunnel tests known as MODFLEX. It consists essentially of a single aluminium alloy spar (load-carrying flexible beam) and four separate aerodynamic sectors, separately connected to the main spar at a single point. The design allows for three active-sector configurations with the purpose of achieving a specified flutter velocity. In support of the design, a finite element (FE) model is described with coupled aerodynamic panels to solve the unsteady aerodynamic using the doublet lattice (DL) method. Active pole placement using the receptance method (RM) is carried out in real-time in a dSPACE environment to increase the flutter velocity by 12%. Experimental tests, carried-out in the wind tunnel facility at the University of Liverpool, are described.

1 Introduction

As part of the EPSRC project *Nonlinear Active Vibration Suppression in Aeroelasticity*, a flexible aeroelastic wing was designed and manufactured to serve as a test rig for the development active control strategies for flutter/vibration suppression and experimental tests. The version considered in this work features a single trailing edge flap to achieve the required control authority.

This paper presents hereinafter a brief literature review related to recent wind tunnel aeroelastic model design developments and the advancements in control strategies for flutter/vibration suppression. In Section 2 the wind tunnel aeroelastic model MODFLEX is presented and compared against the behaviour of the numerical model used in the development of its design. Section 3 describes the control algorithm, based on the receptance method, used to extend the boundary of the flutter velocity V_f. Section 4 illustrates the experimental setup and Section 5 the results.

Over the recent years, as a result of the push given by the NASA Active Flexible Wing (AFW) and Active Aeroelastic Wing (AAW) programs [1, 2], many experimental models have been developed. Heeg at al. [3] designed and tested a wind-tunnel model a 26% geometrically scaled right half-span representation of an F/A-18A featuring four control surfaces; Amiryants et al. [4] developed an experimental platform for the demonstration of the new technical decisions and concepts according to the goals of the European 3AS Project - “Active Aeroelastic Aircraft Structures” [5]. De Gaspari et al. [6] designed, developed and manufacture a forward-swept wind-tunnel aeroelastic wing model with four control surfaces and embedded accelerometers. Heinze et al. [7] developed 1.6 m span high aspect ratio wing (HARW) wind tunnel model with an embedded piezoelectric tab actuator. More recently, Dowell et al. [8] studied the behaviour of a horizontal-tail model with free play.

From the control point of view, the research conducted at the University of Liverpool over the past few years has been aimed to develop linear and nonlinear control strategies for structural dynamics and aeroelastic models. Papatheou et al. [9] implemented the Receptance Method [10] experimentally on a linear 2 degree-of-freedom aeroelastic system to successfully increase the flutter speed by separating pitch and plunge modes via pole-placement. Theoretical work and numerical modelling have primarily been on

controlling smooth and non-smooth nonlinear aeroelastic systems by Da Ronch et al. [11] and Jiffri et al. [12]. Elsewhere, several publications on the application of active control on linear and nonlinear aeroelastic systems have appeared. Amongst them, Singh et al. [13] presents a numerical study on using the RM in a MIMO wing model, Mattaboni et al. [14] developed a control algorithm based on recurrent neural networks for active flutter suppression for a three-surface transport aircraft and Strganac et al. [15] developed and experimentally tested, on the NATA test apparatus, different linear and nonlinear control strategies [16].

2 MODFLEX design

The design approach chosen for MODFLEX follows the one described by Bisplinghoff et al. [17] with the innovation of using 3D printing technologies to achieve the required internal and aerodynamic shapes. Moreover, a modular design has been pursued: the same aeroelastic model can be assembled with between one and four discrete control surfaces or with a morphing surface. Whilst respecting dimensional standard, actuators may be installed internally to the wing structure

The wind tunnel aeroelastic wing is composed by a main spar plus four aerodynamic sectors and a tip sector, as shown in Figure 1. The main specifications of MODFLEX aeroelastic flexible wing are summarized in Table 1.

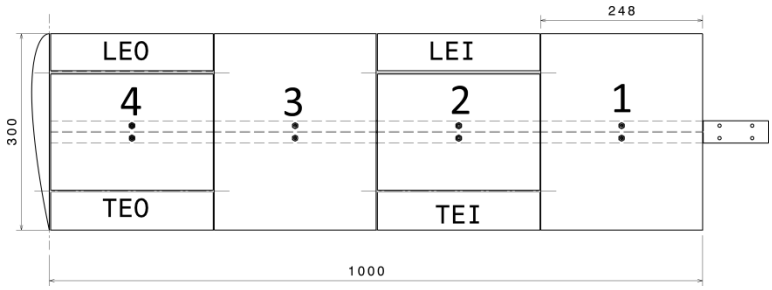

Figure 1: MODFLEX drawing [mm], (b) configuration.

wing data	dimension
wing span	1 m
wing sector	0.248 m
sector chord (c)	0.3 m
aerofoil	NACA 0018
mass axis position	0.5×c
flexural axis position	0.5×c

Table 1: MODFLEX main specifications.

The main spar is made by aluminium alloy and it is the only structural element of the model. By accurately shaping the cross-section of the main spar, the desired flexural, torsional and in-plane stiffnesses have been achieved. Figure 2 depicts the cross section chosen for the aluminium alloy main spar and its dimensions are summarized in Table 2. The cross shape was chosen because it allows an almost independent operation of flexural and torsional rigidity.

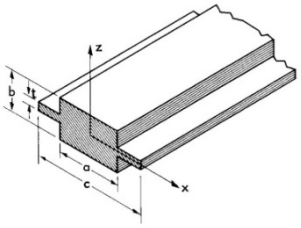

Figure 2: Main spar cross-section.

dimension	mm
a	3
b	17
c	34
t	2

Table 2: Main spar dimensions.

The main spar is covered by four sectors that provide the correct aerodynamic shape. Each sector is connected to the main spar by two pins at the mid span of the sector in order to not alter the stiffness distribution of the overall model. The sectors are 3D-printed and made by ABS. Three-D (3-D) printing was

chosen as the manufacturing technology due to the high level of design flexibility that it allows. The mass centre of gravity and the flexural axis were designed to be coincident on the main spar.

MODFLEX has been designed in order to allocate different control surfaces configurations. Specifically, it is possible to assemble the wind tunnel aeroelastic model as follow:

a) Discrete trailing edge control surface sector as shown in Figure 3. It features a trailing edge outer (TEO) flap located in sector 4 with hinge axis at 0.2×c. The control surface span is equal is to the sector span.

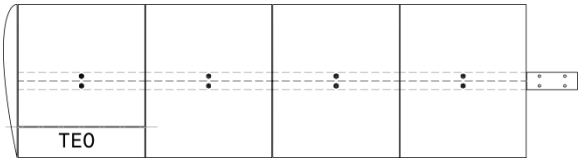

Figure 3: MODFLEX drawing – (a) configuration.

b) Discrete trailing and leading edge outer and inner (TEO, LEO and TEI and LEI - according to NASA terminology [1]) control surface sectors. This configuration features two sectors, numbers 2 and 4, that have both a trailing and a leading edge control surface. The hinge axes are located respectively at 0.2×c and 0.8×c. The control surfaces span is equal to the span of each sector.
c) Morphing sector: this configuration features the sector number 4 designed as a morphing element [18].

In the cases of configurations (a) and (b) the surfaces are actuated by brushless motors embedded within the sectors as shown in Figure 4. Three-D printing manufacturing allows a clean external surface to be achieved.

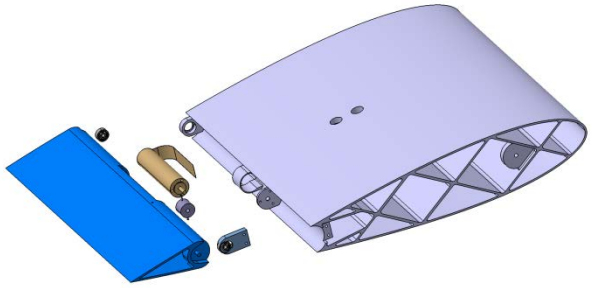

Figure 4: MODFLEX control surface kinematics.

motor data	pn 395588
nominal voltage	24 V
max. continuous torque	15.1 mNm
max. continuous current	2.49 A
stall torque	210 mNm
torque constant	6.39 mNm/A
rotor inertia	1.07 gcm^2

Table 3: Maxon EC 16 Ø16 mm, 60 Watt.

The brushless motor chosen was the current-controlled Maxon EC 16 Ø16 mm, 60 Watt, paired with the encoder MR, Type ML, 512 CPT, 3 Channels, and the driver ESCON 36/3 EC, 2.7/9 A, 10 - 36 VDC . The choice of this motor was due to its relatively high bandwidth, high torque and light weight. The specifications of the motor are presented in Table 3.

Configuration (a), shown in Figure 3, is used in the present work.

2.1 Numerical model

Once the dimensions and the design approach was defined, a numerical model of MODFLEX was produced to drive the development of the experimental model structure. The numerical model is a beam FE model with concentrated masses and 2% structural damping, to which are added aerodynamic panels to solve the unsteady aerodynamic with MD.Nastran DLM. The FE model features four control surfaces that can be locked/unlocked independently. The numerical model was used both to obtain an estimate of the hinge

moment at the control surface - thereby allowing the selection of a suitable actuator - and to forecast the flutter speed while varying the main spar cross sectional properties. Static analysis was carried out showing the self-weight tip displacement to be 35 mm.

2.2 Modal test and experimental-numerical model comparison

A modal test was carried out on the specimen and the results compared with those from the numerical model. The natural frequencies and the relative mode shapes, both numerical and experimental, are summarised in Table 4. The experimental modal test was performed by the impact hammer technique with a web of accelerometers and the Simens.PLM LMS Test.Lab acquisition system.

Mode	Mode Shape	Numerical	Experimental		Error
		Frequency [Hz]	Frequency [Hz]	Damping, ζ [%]	%
1	1^{st} bending mode	3.28	3.22	0.13	1.7
2	1^{st} torsion mode	5.59	5.42	0.94	3.0
3	1^{st} in-plane mode	7.53	7.04	0.27	6.6
4	2^{nd} torsion mode	15.91	15.63	0.70	1.7
5	2^{nd} bending mode	17.87	20.15	0.46	-12.7
6	3^{rd} torsion mode	24.19	23.87	0.52	1.3
7	4^{th} torsion mode	28.59	28.79	0.20	-0.7
8*	3^{rd} bending mode	39.22	-	-	-
9	2^{nd} in-plane mode	44.48	39.46	0.24	11.3
10*	3^{rd} bending mode	-	49.43	0.66	-
11	4^{th} bending mode	106.21	-	-	-

Table 4: Mode shapes and frequencies.

No model updating was performed at this stage of the development.

2.3 Flutter test

The V-f/g (velocity vs. frequency/damping – where the damping g is expressed as $g = -2\zeta$) diagrams, computed with the MD.Nastran SOL145, are depicted by the continuous lines in Figure 5 and show a numerical flutter velocity $V_{f_{numerical}}$ of 14 m/s.

An experimental flutter test was carried out on MODFLEX as well. The model, in the (a) configuration, was positioned in the wind tunnel and with the control surface constrained at the zero position. The wind speed was increased from 10 m/s, with steps of 0.5 m/s, until the model become unstable. The experimental flutter velocity measured was $V_{f_{experimental}} = 12.5$ m/s. The lower value to respect to the numerical prediction is attributed to the models differences also highlighted by the modal analysis. The five- and six-pointed star markers superimposed on Figure 5 show the experimental values for comparison with numerical predictions. The smaller damping values portend a lower flutter velocity for the experimental model.

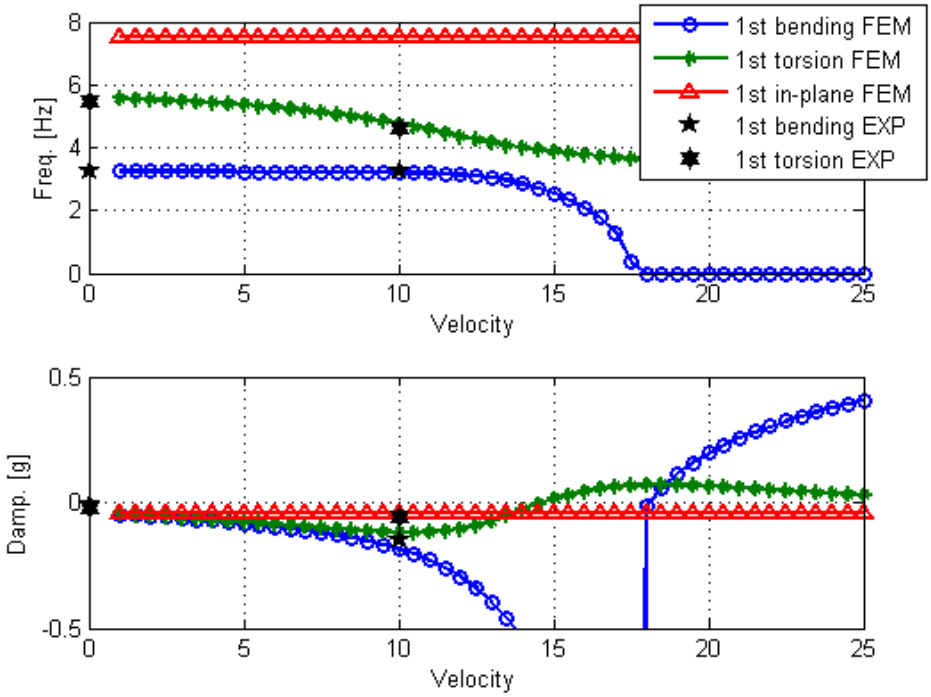

Figure 5: V-f/g (velocity vs. frequency/damping) diagram.

3 Control algorithms

The goal of the control algorithm implemented in this work is to increase the flutter speed by enhancing the damping of the first bending and torsional modes. To achieve this result, a control strategy was developed based on a single-input (TEO flap angular displacement) implementation of the RM. The inputs were wing bending and torsional displacement to be described in Section 4. An inner-loop PID controller was necessary to ensure that the demanded flap deflection was achieved.

3.1 Inner control layer – PID

A PID controller was developed for each control surface. It forms a closed loop between the input current to the brushless motor and the feedback signal from the encoder connected to the motor shaft. This additional control layer was necessary due to the complexity of the transfer function of the actuator itself that cannot be treated as a simple linear relationship. Moreover, the PID on the angular position ensures that, during the modal testing, the structure's input is a proper sinusoidal excitation.

3.2 High-level controller – RM implemented on MODFLEX

The receptance method [10, 19, 20] is applicable to any frequency response function, but is ready understood in terms of receptances. We consider the eigenvalue equation for the $\mathbf{M},\mathbf{C},\mathbf{K}$ system with feedback gains $\mathbf{F},\mathbf{G}$ and control force distribution matrix $\mathbf{B}$. Thus,

$$\left(\lambda_k^2\mathbf{M}+\lambda_k\mathbf{C}+\mathbf{K}\right)\mathbf{w}_k=\mathbf{B}\left(\lambda_k\mathbf{F}^T+\mathbf{G}^T\right)\mathbf{w}_k \qquad (1)$$

where,

$$\mathbf{B}=\begin{bmatrix}\mathbf{b}_1 & \mathbf{b}_2 & \cdots & \mathbf{b}_m\end{bmatrix}\quad \mathbf{F}=\begin{bmatrix}\mathbf{f}_1 & \mathbf{f}_2 & \cdots & \mathbf{f}_m\end{bmatrix}\quad \mathbf{G}=\begin{bmatrix}\mathbf{g}_1 & \mathbf{g}_2 & \cdots & \mathbf{g}_m\end{bmatrix} \tag{2}$$

The RM is a partial pole placement approach whereby the first p poles are to be assigned and the remaining poles, numbered $p+1,\ldots,2n$, are to be retained unchanged. Ram and Mottershead [21] showed that for the multi-input, multi-output (MIMO) case of equation (1) the control gains $\mathbf{F},\mathbf{G}$ are given by the solution of,

$$\begin{bmatrix}\mathbf{P}_1\\ \vdots\\ \mathbf{P}_p\\ \mathbf{Q}_{p+1}\\ \vdots\\ \mathbf{Q}_{2n}\end{bmatrix}\begin{pmatrix}\mathbf{f}_1\\ \vdots\\ \mathbf{f}_m\\ \mathbf{g}_1\\ \vdots\\ \mathbf{g}_m\end{pmatrix}=\begin{pmatrix}\boldsymbol{\alpha}_1\\ \vdots\\ \boldsymbol{\alpha}_p\\ \mathbf{0}\\ \vdots\\ \mathbf{0}\end{pmatrix}\qquad \begin{cases}\mathbf{P}_k=\begin{bmatrix}\mu_k\mathbf{w}_k^T & 0 & \cdots & 0 & \mathbf{w}_k^T & 0 & \cdots & 0\\ 0 & \mu_k\mathbf{w}_k^T & \cdots & 0 & 0 & \mathbf{w}_k^T & \cdots & 0\\ \vdots & \vdots & \ddots & \vdots & \vdots & \vdots & \ddots & \vdots\\ 0 & 0 & \cdots & \mu_k\mathbf{w}_k^T & 0 & 0 & \cdots & \mathbf{w}_k^T\end{bmatrix}\\ \mathbf{Q}_k=\begin{bmatrix}\lambda_k\mathbf{v}_k^T & 0 & \cdots & 0 & \mathbf{v}_k^T & 0 & \cdots & 0\\ 0 & \lambda_k\mathbf{v}_k^T & \cdots & 0 & 0 & \mathbf{v}_k^T & \cdots & 0\\ \vdots & \vdots & \ddots & \vdots & \vdots & \vdots & \ddots & \vdots\\ 0 & 0 & \cdots & \lambda_k\mathbf{v}_k^T & 0 & 0 & \cdots & \mathbf{v}_k^T\end{bmatrix}\end{cases} \tag{3}$$

where,

$$\mathbf{w}_k=\alpha_{k,1}\mathbf{r}_{k,1}+\alpha_{k,2}\mathbf{r}_{k,2}+\ldots+\alpha_{k,m}\mathbf{r}_{k,m};\quad k=1,2,\ldots,p \tag{4}$$

$$\mathbf{r}_{k,j}=\mathbf{H}(\mu_k)\mathbf{b}_j;\quad j=1,2,\ldots,m \tag{5}$$

the assigned and retained poles are denoted by $\mu_{k=1,2,\ldots,p}$ and $\lambda_{k=p+1,p+2,\ldots,2n}$ respectively and $\mathbf{v}_{k=p+1,p+2,\ldots,2n}$ denotes the retained eigenvectors. Judicious choice of $\alpha_{k,j}\ (k=1,2,\ldots,p;\ j=1,2,\ldots,m)$ determines the eigenvectors of the assigned modes via equation (4). It is seen that the method does not require knowledge of the matrices $\mathbf{M},\mathbf{C},\mathbf{K}$ directly. It requires the frequency response function $\mathbf{H}(\mu_k)$ at the locations of the poles.

4 Experimental setup and testing

The experimental campaign was carried out in the low speed wind tunnel of The University of Liverpool. This facility features a test section of 1.2×0.6×1.0 m and a maximum airspeed of 20 m/s. The wing model is fully constrained at the built-in end. The MODFLEX configuration adopted for the work here presented is configuration (a) featuring a single trailing edge control surface in sector number 4.

The encoder connected to the brushless motor's shaft that actuates the control surfaces provides the feedback signal for the inner control loop.

The high-level controller instead, is implemented by using the feedback signals provided by two laser sensors (Keyence LK-500) measuring the displacement of two points located in the third sector of MODFLEX at 0.25×c and 0.75×c respectively. A filtering of the displacement signals was required; specifically, a second-order Butterworth low-pass filter with cut-off frequency 15 Hz was used. Figure 6 shows on the left the configuration chosen for the present work and the position of the laser displacement sensors, Figure 7 shows the model installed in the wind tunnel section.

The experimental setup block diagram is depicted in the right-hand-side of Figure 6. The real time acquisition system dSPACE is the environment in which the controllers are implemented. The inner-loop acquires the digital encoder signal, implements the PID and produces the voltage output to the brushless motor's diver that provides current to the motor. The outer-loop acquires the analog signal from the two laser displacement sensors and computes the required control surface angular displacement, this value is then transmitted, through the inner-loop, to the actuator.

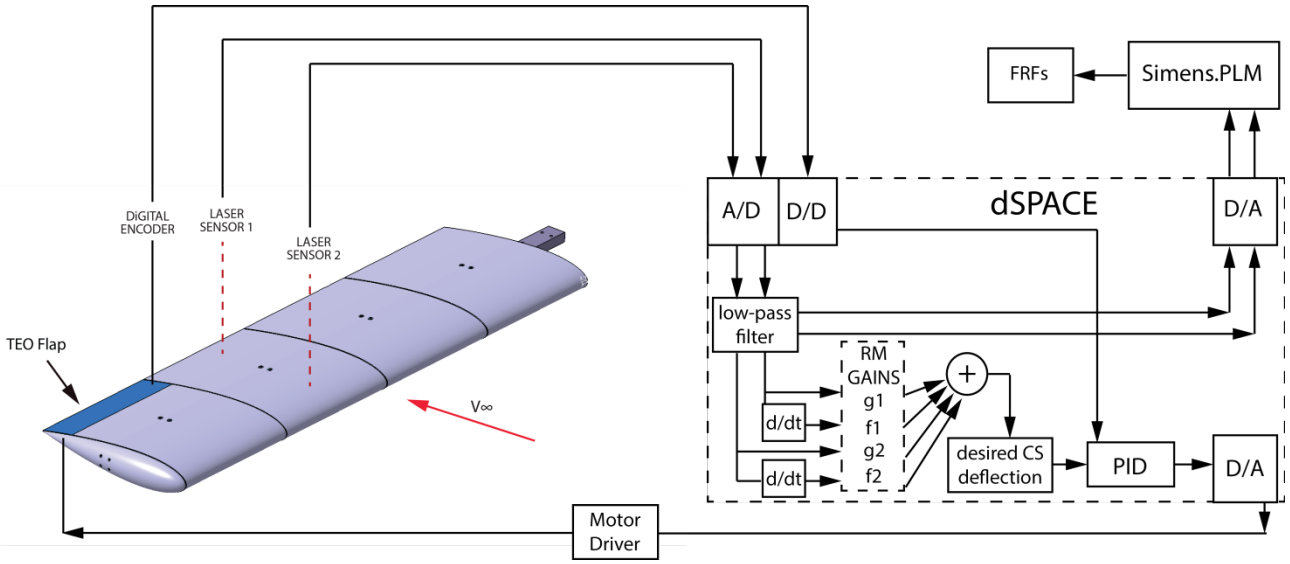

Figure 6: MODFLEX experimental setup & block diagram.

Figure 7: MODFLEX wind tunnel model.

4.1 Experimental implementation of the Receptance Method

As explained in Section 3.2, the preliminary information necessary to implement the RM are the FRFs. The model is positioned in the wind tunnel with a freestream of 10 m/s and excited with a stepped sine oscillation of the TEO flap. The signals from the two laser sensors are acquired by using the Simens.PLM LMS Test.Lab.

The procedure for applying the receptance method is as follows:

- Measure the open loop input-output FRFs over the frequency range of interest, from 2 to 6 Hz – the input is the TEO flap angular displacement measured using the Maxon digital encoder MR, that features 512 CPT and the outputs are the laser sensor measurements.
- Fit SIMO rational fraction polynomials to the measured FRFs and obtain input-output transfer functions.
- Select force distribution vector $\mathbf{b}_1(s)$ for the configuration (a) – single TEO – $\mathbf{b}_1(s)=1$.
- Assign frequency and damping of the poles - specifically, the first bending and torsion modes. The value of the frequencies were kept unchanged and the damping was increased by 20 and 30 % respectively,

$$\mu_{1,2} = -1.76 \cdot 1.2 \pm 3.25i$$
$$\mu_{3,4} = -1.09 \cdot 1.3 \pm 4.65i$$

- Apply the Receptance Method (equation (3)) to obtain unknown gains, $\mathbf{g}_1 = -24.67, \mathbf{g}_2 = 34.46$ and $\mathbf{f}_1 = 0.357, \mathbf{f}_2 = -0.283$.
- The control algorithm was developed in Simulink and implemented in dSPACE. As shown on the right-hand-side of Figure 6, the two displacement signals were acquired and differentiated once to obtain the velocities. The four signals, third sector front and rear displacements and velocities, were then multiplied respectively by the gains **g** and **f** computed offline. The resultant signals were added together and passed to the inner loop where the PID (control surface encoder angular position – supplied voltage to the brushless motor) was implemented. The final signal was transmitted to the motor driver and then to the actuator itself.

4.2 Close-loop modal test

The aeroelastic model coupled with the active controller was tested in a closed loop modal analysis. The MODFLEX was installed in the wind tunnel in the same configuration and conditions used for the open loop input-output FRFs evaluation described previously with active TEO flap and 10 m/s airspeed. Stepped sine excitation signal was supplied to the flap with the same frequency range, amplitude and number of cycles used for the open-loop measurements. The control signal, generated by the feedback algorithm based on the RM gains, described above, was then added to the excitation signal and the response acquired using the Simens.PLM LMS Test.Lab. The values of frequencies and damping were computed by the modal parameter estimation technique PolyMAX [22] and compared to the open-loop values.

4.3 Close-loop flutter test

The experimental flutter test described in Section 2.3 was performed again with the close loop controller engaged. Starting form 10 m/s, the wind speed was increased, with steps of 0.5 m/s, until the model became unstable. The closed loop experimental flutter velocity recorded was $V_{f_{CL,experimental}} = 14$ m/s.

5 Results

Figure 8 and Figure 9 show the FRFs between the two displacement sensors and the angular flap deflection, in the open – continuous line - and closed – dashed line - loop situation. As described in Section 4.1, the value of the two frequencies was kept unchanged while the controller was designed to act on the damping. The different trend between Figure 8 and Figure 9 phase diagrams is due to the fact that, if for the bending mode the displacement ahead and aft the flexural axis of the wing is the same, for the torsion mode, it is opposite.

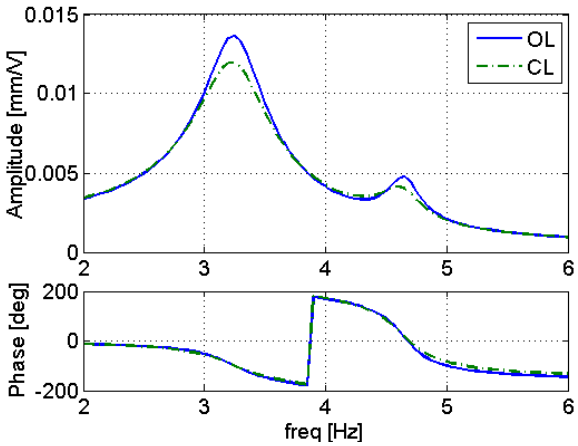

Figure 8: Displacement laser sensor 1.

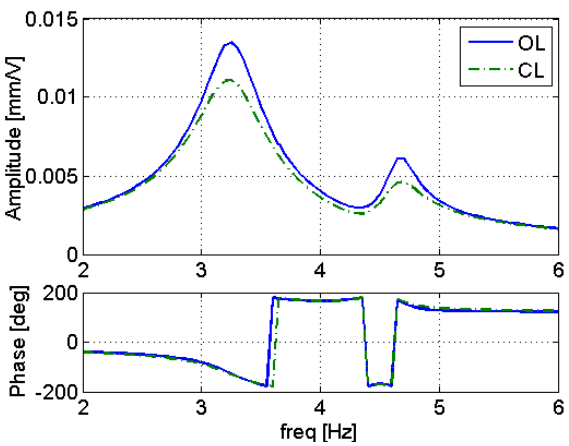

Figure 9: Displacement laser sensor 2.

The numerical differences between the open and the close loop tests are presented in Table 5, the values of the frequencies can be considered almost unchanged while the damping of the first bending and torsion modes are increased by 17.7 % and 33.8 % respectively. These values are obtained by averaging the two FRFs.

mode shape	open loop		closed loop	
	frequency [Hz]	damping, ζ [%]	frequency [Hz]	damping, ζ [%]
1st bending	3.25	7.84	3.24	9.23
1st torsion	4.65	2.90	4.63	3.88

Table 5: first bending and torsion modes comparison, airspeed 10 m/s.

The flutter velocity V_f was increased by the required 12 % from 12.5 to 14 m/s.

6 Conclusions

The Receptance Method applied to the present work proved to be a suitable means of extending the model flutter envelope without having to reconstruct a numerical state-space model of the aeroelastic setup. Moreover, if the poles are assigned without exceeding the control surface authority, the prescribed values are closely achieved. Further development will see the experimental testing of the configuration (b), multiple leading and trailing edge control surfaces and the implementation of the Receptance Method in its full MIMO version.

Acknowledgements

This research was funded by EPSRC grant EP/J004987/1 under the project entitled *Nonlinear Active Vibration Suppression in Aeroelasticity*.

References

[1] E. W. Pendleton, D. Bessette, P. B. Field, G. D. Miller, K. E. Griffin, *Active Aeroelastic Wing Flight Research Program: Technical Program and Model Analytical Development*, Journal of Aircraft, Vol. 37, No. 4, 2000, pp. 554–561.

[2] B. Perry, III, S. R. Cole, G. D. Miller, *Summary of an Active Flexible Wing program*, Journal of Aircraft, Vol. 32, No. 1, 1995, pp. 10–15.

[3] J. Heeg, V. Spain, J. Florance, C. Wieseman, T. Ivanco, J. De Moss, W. Silva, A. Panetta, P. Lively, V. Tumwa, *Experimental Results from the Active Aeroelastic Wing Wind Tunnel Test Program*, in *46th AIAA/ASME/ASCE/AHS/ASC Structures, Structural Dynamics and Materials Conference, Austin, Texas, 2005 April 18-21*, Austin (2005), pp. 1–16.

[4] G. A. Amiryants, Y. M. Mullov, S. V Shalaev, M. C. Zichenkov, *Design, manufacture and wind tunnel testing of the multifunctional European Research Aeroelastic Model (EuRAM)*, in *European Conference for Aerospace Sciences (EUCASS)*, 2005.

[5] V. V Simpson J., Anguita-Delgado L., Kawiecki G., Nilsson B., *Review of the European Research Project 'Active Aeroelastic Aircraft Structures (3AS)'*, in *European Conference for Aerospace Sciences (EUCASS)*, 2005.

[6] A. De Gaspari, S. Ricci, L. Riccobene, A. Scotti, *Active Aeroelastic Control Over a Multisurface Wing: Modeling and Wind-Tunnel Testing*, AIAA Journal, Vol. 47, No. 9, pp. 1995–2010, Sep. 2009.

[7] S. Heinze, M. Karpel, *Analysis and Wind Tunnel Testing of a Piezoelectric Tab for Aeroelastic Control Applications*, Journal of Aircraft., Vol. 43, No. 6, 2006, pp. 1799–1804.

[8] D. Tang, E. H. Dowell, *Computational/Experimental Aeroelastic Study for a Horizontal-Tail Model with Free Play*, AIAA Journal, Vol. 49, No. 11, 2011, pp. 341–352.

[9] E. Papatheou, N. D. Tantaroudas, A. Da Ronch, J. E. Cooper, J. E. Mottershead, A. Da Ronch, *Active control for flutter suppression: an experimental investigation*, in *International Forum on Aeroelasticity and Structural Dynamics (IFASD), Bristol, United Kingdom, 2013 June 24-26*, United Kingdom (2013), pp. 1-14.

[10] J. E. Mottershead, Y. M. Ram, *Receptance Method in Active Vibration Control*, AIAA Journal, Vol. 45, No. 3, 2007, pp. 562–567.

[11] A. Da Ronch, N. D. Tantaroudas, S. Jiffri, J. E. Mottershead, *A Nonlinear Controller for Flutter Suppression: from Simulation to Wind Tunnel Testing*, in *55th AIAA/ASMe/ASCE/AHS/SC Structures, Structural Dynamics, and Materials Conference, National Harbor, Maryland*, Maryland (2014), pp. 1–19.

[12] S. Jiffri, P. Paoletti, J. E. Mottershead, *Feedback Linearization in Systems with Nonsmooth Nonlinearities*, Journal of Guidance, Control, and Dynamics, Vol. 39, No. 4, 2016, pp. 814–825.

[13] K. V Singh, L. A. Mc Donough, R. Kolonay, J. E. Cooper, *Receptance-Based Active Aeroelastic Control Using Multiple Control Surfaces*, Journal of Aircraft, Vol. 51, No. 1, 2014, pp. 335–342.

[14] M. Mattaboni, G. Quaranta, P. Mantegazza, *Active Flutter Suppression for a Three-Surface Transport Aircraft by Recurrent Neural Networks*, Journal of Guidance, Control, and Dynamics, Vol. 32, No. 4, 2009, pp. 1295–1307.

[15] J. J. Block, T. W. Strganac, *Applied Active Control for a Nonlinear Aeroelastic Structure*, Journal of Guidance, Control, and Dynamics, Vol. 21, No. 6, 1998, pp. 838–845.

[16] Y. S. Lee, G. Kerschen, D. M. McFarland, W. J. Hill, C. Nichkawde, T. W. Strganac, L. A. Bergman, A. F. Vakakis, *Suppressing Aeroelastic Instability Using Broadband Passive Targeted Energy Transfers, Part 2: Experiments*, AIAA Journal, Vol. 45, No. 10, 2007, pp. 2391–2400.

[17] R. L. Bisplinghoff, H. Ashley, R. L. Halfman, *Aeroelasticity*, Aeronautic. New York, NY: Dover Publications, 1996.

[18] S. Fichera, S. Jiffri, X. Wei, J. E. Mottershead, *High Bandwidth Morphing Aerofoil*, in *ICAST2014: 25th International Conference on Adaptive Structures and Technologies, the Hague, The Netherlands, 2014 October 6-8*, The Hague (2014).

[19] M. Ghandchi Tehrani, R. N. R. Elliott, J. E. Mottershead, *Partial pole placement in structures by the method of receptances: Theory and experiments*, Journal of Sound and Vibration, Vol. 329, No. 24, 2010, pp. 5017–5035.

[20] E. Papatheou, X. Wei, S. Jiffri, M. Prandina, M. G. Tehrani, S. Bode, K. V. Singh, J. E. Mottershead, J. Cooper, *Flutter control using vibration test data: theory, rig design and preliminary results*, in *International Seminar on Modal Analysis (ISMA2012), Leuven, Belgium*, Belgium (2012).

[21] Y. M. Ram, J. E. Mottershead, *Multiple-input active vibration control by partial pole placement using the method of receptances*, Mechanical Systems and Signal Processing, Vol. 40, No. 2, 2013, pp. 1–9.

[22] B. Peeters, G. Lowet, H. Van Der Auweraer, J. Leuridan, L. M. S. International, *A New Procedure for Modal Parameter Estimation*, Sound and Vibration, Vol. 38, 2004, pp. 24–28.